Specific heat (1.2–108 K) and thermal expansion (4.4–297 K) measurements of the 3*d* heavy-fermion compound LiV_2O_4

D. C. Johnston, C. A. Swenson, and S. Kondo
Ames Laboratory and Department of Physics and Astronomy, Iowa State University, Ames, Iowa 50011
(Received 27 May 1998)

Specific heat $C_p(T)$ measurements of the heavy-fermion normal-spinel structure compound LiV_2O_4 were carried out using a heat-pulse calorimeter over the temperature T range from 1.2 to 108 K. The electronic specific heat $C_e(T)$ of LiV_2O_4 is extracted from the $C_p(T)$ data using the lattice contribution obtained for $LiTi_2O_4$, a superconductor with $T_c=11.8$ K. The electronic specific heat coefficient $\gamma(T)\equiv C_e(T)/T$ of LiV_2O_4 is found to be 0.42 and 0.43 J/mol K^2 at $T=1$ K for two different high-magnetic-purity samples, respectively. $\gamma(T)$ decreases rapidly with increasing temperature from 4 to 30 K and then decreases much more slowly from 0.13 J/mol K^2 at 30 K to 0.08 J/mol K^2 at 108 K. The $C_e(T)$ of the first of the above two LiV_2O_4 samples is compared with theoretical predictions for the spin $S=1/2$ Kondo model, a generic Fermi liquid model, and an antiferromagnetically coupled quantum-disordered metal. Each of these theories can adequately describe the T dependence of C_e in the Fermi liquid regime at low (~1–10 K) temperatures, consistently yielding a large extrapolated $\gamma(0)=428(3)$ mJ/mol K^2. However, none of these theories describes $C_e(T)$ from ~10 K to 108 K. Our $C_e(T)$ data are also in severe disagreement with the magnetic specific heat of the spin $S=1/2$ Heisenberg model, calculated above ~40 K for the V sublattice of the spinel structure. Thermal expansion measurements of LiV_2O_4 were carried out from 4.4 to 297 K using a differential capacitance dilatometer. Strong increases in the thermal expansion coefficient and Grüneisen parameter Γ are found below ~20 K, confirming the results of Chmaissem *et al.* [Phys. Rev. Lett. **79**, 4866 (1997)] obtained using neutron diffraction. We estimate $\Gamma(0)\approx 11.4$, which is intermediate between those of conventional metals and *f*-electron heavy-fermion compounds. [S0163-1829(99)04404-5]

I. INTRODUCTION

Heavy-fermion (HF) and related intermediate-valence (IV) behaviors are ubiquitous in metallic *f*-electron systems containing lanthanide or actinide ($\equiv M$) atoms with unstable valence.[1] The HF materials are typically intermetallic compounds containing Ce, Yb, or U ions and are characterized at the lowest temperatures T by a large and nearly T-independent spin susceptibility $\chi(T\rightarrow 0)$ $\sim 10^{-2}$ $cm^3/(mol\ M)$ and an extraordinarily large nearly T-independent electronic specific heat coefficient $\gamma(T\rightarrow 0)$ ~ 1 J/(mol M) K^2, where $\gamma(T)\equiv C_e(T)/T$ and $C_e(T)$ is the electronic contribution to the measured specific heat at constant pressure $C_p(T)$. Large quasiparticle effective masses m^* of ~100–1000 electron masses m_e have been inferred from $\gamma(0)$ for the HF compounds and smaller values for the IV materials. The normalized ratio of $\chi(0)$ to $\gamma(0)$, the Sommerfeld-Wilson ratio[2] R_W, is on the order of unity in HF and IV materials as in conventional metals, and is given by $R_W=\pi^2 k_B^2\chi(0)/3\mu_{eff}^2\gamma(0)$, where k_B is Boltzmann's constant and μ_{eff} is the effective magnetic moment of the Fermi liquid quasiparticles. For quasiparticles with (effective) spin $S=1/2$, one obtains

$$R_W=\frac{4\pi^2 k_B^2\chi(0)}{3g^2\mu_B^2\gamma(0)}, \tag{1}$$

where g is the g factor of the quasiparticles and μ_B is the Bohr magneton. Since $R_W\sim 1$ in many of the HF and IV compounds, χ and C_e at low temperatures are both probing the same low-energy heavy-quasiparticle spin excitations. With increasing T in the heaviest-mass systems, $\chi(T)$ crosses over to local-moment behavior and γ decreases rapidly, on a temperature scale of ~0.3–30 K.

Heavy-fermion behaviors are not expected for *d*-electron compounds because of the much larger spatial extent of *d* orbitals than of *f* orbitals and the resulting stronger hybridization with conduction-electron states. Recently, however, in collaboration with other researchers, we have documented HF behaviors, characteristic of those of the heaviest mass *f*-electron HF systems, in the metallic[3] transition-metal oxide compound LiV_2O_4 using $C_p(T)$,[4] $\chi(T)$,[4,5] ^{7}Li and ^{51}V NMR,[4,6] muon spin relaxation (μSR),[4,7] and 4–295 K crystallography[4,5,8] measurements. Independent crystallography and $\chi(T)$ measurements[9,10] and NMR measurements[10–12] were reported nearly simultaneously by other groups, with similar results. LiV_2O_4 has the face-centered-cubic normal-spinel structure (space group $Fd\bar{3}m$),[13] and is formally a $d^{1.5}$ system. The Li atoms occupy tetrahedral holes and the V atoms octahedral holes in a nearly cubic-close-packed oxygen sublattice, designated as $Li[V_2]O_4$. The $C_e(T)$ is extraordinarily large for a transition-metal compound, $\gamma(1\ K)\approx 0.42$ J/mol K^2, decreasing rapidly with T to ~0.1 J/mol K^2 at 30 K.[4] As discussed extensively in Refs. 4 and 5, from ~50–100 K to 400 K, $\chi(T)$ shows a Curie-Weiss-like [$\chi=C/(T-\theta)$] behavior corresponding to antiferromagnetically coupled ($\theta=-30$ to -60 K) vanadium local magnetic moments with $S=1/2$ and $g\approx 2$, but static magnetic ordering does not occur above 0.02 K in magnetically pure LiV_2O_4, and superconductivity is not observed above 0.01 K.

TABLE I. Lattice parameter a_0 and structural [f_{imp} (str)] and magnetic [f_{imp} (mag)] impurity concentrations for the LiV_2O_4 samples studied in this work (Ref. 5).

Sample No.	2	3	4A	5	6
Lattice parameter (Å)	8.23997(4)	8.24100(15)	8.24705(29)	8.24347(25)	8.23854(11)
Impurity phase	V_2O_3	pure	V_2O_3	V_2O_3	V_3O_5
f_{imp} (str) (mol %)	1.83	<1	1.71	<1	2.20
f_{imp} (mag) (mol %)	0.22(1)	0.118(2)	0.77(2)	0.472(8)	0.0113(6)

To our knowledge, in addition to LiV_2O_4 the only other stoichiometric transition-metal spinel-structure oxide which is metallic to low temperatures is the normal-spinel compound $LiTi_2O_4$.[14–17] In contrast to LiV_2O_4, this compound becomes superconducting at $T_c \leqslant 13.7$ K (Refs. 14 and 18) and has a comparatively T-independent and small $\chi(T)$ from T_c up to 300 K.[14,19–21] The resistivity of thin films at 15 K is $(4.3–8.8)\times 10^{-4}$ Ω cm.[22] The spinel system $Li_{1+x}Ti_{2-x}O_4$ with cation occupancy $Li[Li_xTi_{2-x}]O_4$ exists from $x=0$ to $x=1/3$;[14,15,17] for $x=1/3$,[23] the oxidation state of the Ti is $+4$ and the compound is a nonmagnetic insulator. A zero-temperature superconductor-insulator transition occurs at $x \sim 0.1–0.2$.[14,19,20]

In this paper, we report the details of our $C_p(T)$ measurements on LiV_2O_4 and of the data analysis and theoretical modeling. We have now obtained data to 108 K, which significantly extends our previous high-temperature limit of 78 K.[4] We also present complementary linear thermal expansion $\alpha(T)$ measurements on this compound from 4.4 to 297 K. We will assume that $C_p(T)$ can be separated into the sum of electronic and lattice contributions,

$$C_p(T) = C_e(T) + C^{lat}(T), \tag{2a}$$

$$C_e(T) \equiv \gamma(T)T. \tag{2b}$$

In Ref. 4, we reported $C_p(T)$ measurements up to 108 K on $Li_{4/3}Ti_{5/3}O_4$ which were used to estimate $C^{lat}(T)$ in LiV_2O_4 so that $C_e(T)$ could be extracted according to Eq. (2a). In the present work, we report $C_p(T)$ up to 108 K for $LiTi_2O_4$, compare these data with those for $Li_{4/3}Ti_{5/3}O_4$, and obtain therefrom what we believe to be a more reliable estimate of $C^{lat}(T)$ for LiV_2O_4. The experimental details are given in Sec. II. An overview of our $C_p(T)$ data for LiV_2O_4, $LiTi_2O_4$, and $Li_{4/3}Ti_{5/3}O_4$ is given in Sec. III A. Detailed analyses of the data for the $Li_{1+x}Ti_{2-x}O_4$ compounds and comparisons with literature data are given in Sec. III B, in which we also estimate $C^{lat}(T)$ for LiV_2O_4. The $C_e(T)$ and electronic entropy $S_e(T)$ for LiV_2O_4 are derived in Sec. III C. The $\alpha(T)$ measurements are presented in Sec. IV and compared with the $C_p(T)$ results and lattice parameter data versus temperature obtained from neutron diffraction measurements by Chmaissem *et al.*[8] From the combined $\alpha(T)$ and $C_p(T)$ measurements on the same sample, we derive the Grüneisen parameter from 4.4 to 108 K and estimate the value at $T=0$. Theoretical modeling of the $C_e(T)$ data for LiV_2O_4 is given in Sec. V. Since the electrical resistivity data for single crystals of LiV_2O_4 indicate metallic behavior from 4 K to 450 K,[3] we first discuss the Fermi liquid description of this compound and derive the effective mass and other parameters for the current carriers at low temperatures in Sec. V A. This is followed by a more general discussion of the FL theory and its application to LiV_2O_4 at low T. In Sec. V B we compare the predictions of Zülicke and Millis[24] for a quantum-disordered antiferromagnetically coupled metal with our $C_e(T)$ results for LiV_2O_4. The isolated $S=1/2$ impurity Kondo model predicts FL behavior at low temperatures and impurity local moment behavior at high temperatures. Precise predictions for the $\chi(T)$ and $C_e(T)$ have been made for this model, and we compare our $C_e(T)$ data with those predictions in Sec. V C. In Sec. V D we consider a local moment model in which the magnetic specific heat of the B sublattice of the $A[B_2]O_4$ spinel structure for spins $S=1/2$ and $S=1$ per B ion is given by a high-temperature series expansion and the predictions compared with the $C_e(T)$ data for LiV_2O_4. A summary and concluding remarks are given in Sec. VI. Unless otherwise noted, a ''mol'' refers to a mole of formula units.

II. EXPERIMENTAL DETAILS

Polycrystalline LiV_2O_4 samples were prepared using conventional ceramic techniques described in detail elsewhere, where detailed sample characterizations and magnetic susceptibility results and analyses are also given.[5] A few of these results relevant to the present measurements, analyses, and modeling are given in Table I.

Polycrystalline $LiTi_2O_4$ and $Li_{4/3}Ti_{5/3}O_4$ samples were synthesized using solid-state reaction techniques.[14] TiO_2 (Johnson Matthey, 99.99%) was dried under a pure oxygen stream at 900 °C before use. This was mixed with Li_2CO_3 (Alfa, 99.999%) in an appropriate ratio to produce either $Li_{4/3}Ti_{5/3}O_4$ or a precursor ''$LiTiO_{2.5}$'' for $LiTi_2O_4$. The mixtures were then pressed into pellets and heated at 670 °C in an oxygen atmosphere for ≈1 day. The weight loss due to release of CO_2 was within 0.04 wt % of the theoretical value for $LiTiO_{2.5}$. However, for $Li_{4/3}Ti_{5/3}O_4$ additional firings at higher temperatures (up to 800 °C), after being reground and repelletized, were necessary. $LiTi_2O_4$ was prepared by heating pressed pellets of a ground mixture of the $LiTiO_{2.5}$ precursor and Ti_2O_3 in an evacuated and sealed quartz tube at 700 °C for 1 week and then air cooling. The Ti_2O_3 was prepared by heating a mixture of TiO_2 and titanium metal powder (Johnson Matthey) at 1000 °C for 1 week in an evacuated and sealed quartz tube.

Powder x-ray diffraction data were obtained using a Rigaku diffractometer (Cu $K\alpha$ radiation) with a curved graphite crystal monochromator. Rietveld refinements of the data were carried out using the program ''Rietan 97 ('beta' version).''[25] The x-ray data for our sample of $Li_{4/3}Ti_{5/3}O_4$ showed a nearly pure spinel phase with a trace of TiO_2

TABLE II. Characteristics of $LiTi_2O_4$ and $Li_{4/3}Ti_{5/3}O_4$ samples. Abbreviations: a_0 is the lattice parameter, u the oxygen parameter, γ the electronic specific heat coefficient, θ_0 the zero-temperature Debye temperature, T_c and ΔT_c the superconducting transition temperature and transition width, and ΔC_p the specific heat jump at T_c.

a_0 (Å)	u	γ (mJ/mol K^2)	θ_0 (K)	T_c (K)	ΔT_c (K)	$\Delta C_p/\gamma T_c$ (mJ/mol K^2)	Ref.
			$LiTi_2O_4$				
8.4033(4)	0.2628(8)	17.9(2)	700(20)	11.8	$\lesssim$0.2	1.75(3)	This work
8.4033(1)	0.26275(5)						16
8.41134(1)	0.26260(4)						17
8.407		21.4	685	11.7	1.2	1.59	28
		22.0	535	12.4	0.32	1.57	20
	0.26290(6) (300 K)						21
	0.26261(5) (6 K)						21
			$Li_{4/3}Ti_{5/3}O_4$				
8.3589(3)	0.2625(3)	0.	725(20)				This work
8.35685(2)	0.26263(3)						17
8.359		0.	610				28
		0.05	518				20

(rutile) impurity phase. The two-phase refinement, assuming the cation distribution $Li[Li_{1/3}Ti_{5/3}]O_4$, yielded the lattice a_0 and oxygen u parameters of the spinel phase 8.3589(3) Å and 0.2625(3), respectively; the concentration of TiO_2 impurity phase was determined to be 1.3 mol %. The $LiTi_2O_4$ sample was nearly a single-phase spinel structure but with a trace of Ti_2O_3 impurity. A two-phase Rietveld refinement assuming the normal-spinel cation distribution yielded the spinel phase parameters $a_0=8.4033(4)$ Å and $u=0.2628(8)$, and the Ti_2O_3 impurity phase concentration <1 mol %. Our crystal data are compared with those of Cava *et al.*[16] and Dalton *et al.*[17] in Table II.

The $C_p(T)$ measurements were done on samples from four different batches of LiV_2O_4 using a conventional heat-pulse calorimeter, with Apeizon-N grease providing contact between the sample and the copper tray.[26] Additional $C_p(T)$ data were obtained up to 108 K on 0.88 g of the isostructural nonmagnetic insulator spinel compound $Li_{4/3}Ti_{5/3}O_4$, containing only maximally oxidized Ti^{+4}, and 3.09 g of the isostructural superconductor $LiTi_2O_4$ to obtain an estimate of the background lattice contribution. A basic limitation on the accuracy of these C_p data, except for LiV_2O_4 below 15 K, was the relatively small (and sample-dependent) ratios of the heat capacities of the samples to those associated with the tray (the ''addenda''). For LiV_2O_4 sample 6, this ratio decreased from 40 near 1 K to 1.0 at 15 K to a relatively constant 0.2 above 40 K. For the superconducting $LiTi_2O_4$ sample, this ratio was 0.45 just above T_c ($=11.8$ K), and increased to 0.65 at 108 K. For the nonmagnetic insulator $Li_{4/3}Ti_{5/3}O_4$ sample, this ratio varied from 0.03 to 0.12 to 0.2 at 8, 20, and 108 K, respectively. These factors are important since small ($\pm 0.5\%$) systematic uncertainties in the addenda heat capacity can have differing effects on the $C_p(T)$ measured for the different samples, even though the precision of the raw heat capacity measurements (as determined from fits to the data) is better than 0.25%.

The linear thermal expansion coefficient of LiV_2O_4 sample 6 was measured using a differential capacitance dilatometer.[26,27] All data were taken isothermally (T constant to 0.001 K). The absolute accuracy of the measurements is estimated to be better than 1%.

III. SPECIFIC HEAT MEASUREMENTS

A. Overview

An overview of our $C_p(T)$ measurements on LiV_2O_4 sample 2, run 2 (1.26–78 K), sample 6 (1.16–108 K), and $LiTi_2O_4$ and $Li_{4/3}Ti_{5/3}O_4$ up to 108 K, is shown in plots of $C_p(T)$ and $C_p(T)/T$ in Figs. 1(a) and 1(b), respectively. Our data for $LiTi_2O_4$ and $Li_{4/3}Ti_{5/3}O_4$ are generally in agreement with those of McCallum *et al.*[28] which cover the range up to $\sim$25 K. For $LiTi_2O_4$ above $T_c=11.8$ K (see below) and for $Li_{4/3}Ti_{5/3}O_4$, one sees from Fig. 1(a) a smooth monotonic increase in C_p up to 108 K. From Fig. 1(b), the C_p of the nonmagnetic insulator $Li_{4/3}Ti_{5/3}O_4$ is smaller than that of metallic $LiTi_2O_4$ up to $\sim$25 K, is larger up to $\sim$45 K, and then becomes smaller again at higher temperatures. Since $C_e=0$ in $Li_{4/3}Ti_{5/3}O_4$ and $C_e(T)$ in $LiTi_2O_4$ cannot be negative, it follows from Eq. (2a) that $C^{lat}(T)$ and hence the lattice dynamics are significantly different in $LiTi_2O_4$ compared with $Li_{4/3}Ti_{5/3}O_4$. The data for LiV_2O_4 in Fig. 1(b) are shifted upwards from the data for the Ti spinels, with a strong upturn in $C_p(T)/T$ below $\sim$25 K. These data indicate a very large $\gamma(T\rightarrow 0)$. Comparison of $C_p(T)/T$ for LiV_2O_4 and $LiTi_2O_4$ at the higher temperatures >30 K indicates that a large $\gamma(T)$ persists in LiV_2O_4 up to our maximum measurement temperature of 108 K. In the following, we begin our analyses with the data for the $Li_{1+x}Ti_{2-x}O_4$ compounds because we extract a lattice specific heat from these materials as a reference for LiV_2O_4.

B. $Li_{1+x}Ti_{2-x}O_4$

In the present paper, our $C_p(T)$ data for $LiTi_2O_4$ and $Li_{4/3}Ti_{5/3}O_4$ are most important for determining the lattice

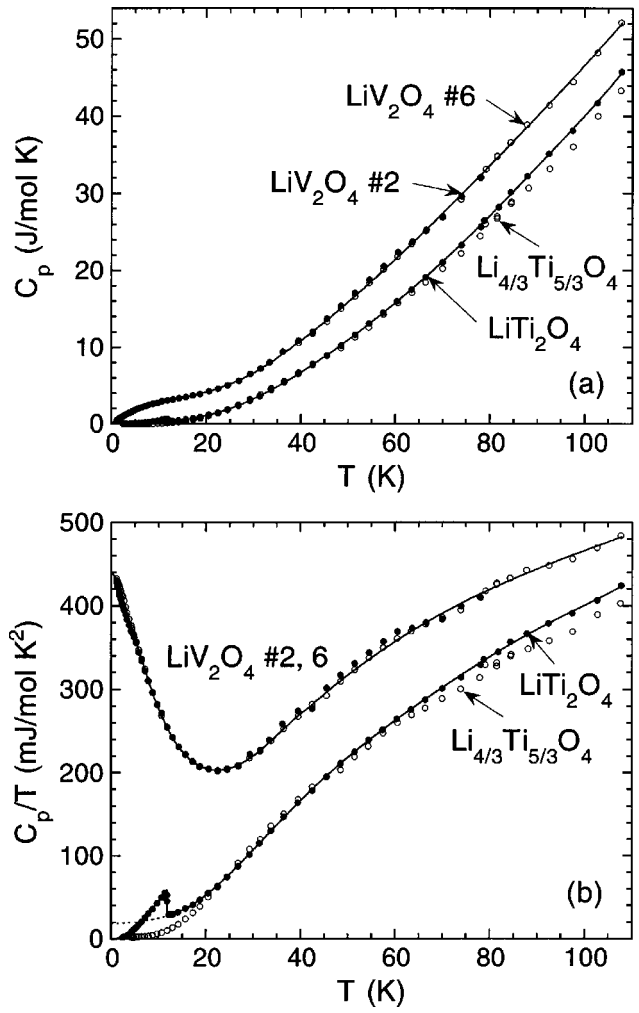

FIG. 1. Overview of the molar specific heat C_p (a) and C_p/T (b) vs temperature T for LiV_2O_4 samples 2 (●) and 6 (○) and the reference compounds $LiTi_2O_4$(●), a metallic superconductor, and $Li_{4/3}Ti_{5/3}O_4$(○), a nonmagnetic insulator. The solid curves are polynomial fits to the data for LiV_2O_4 sample 6 and $LiTi_2O_4$. The dashed curve in (b) is the inferred normal state C_p/T below T_c for $LiTi_2O_4$.

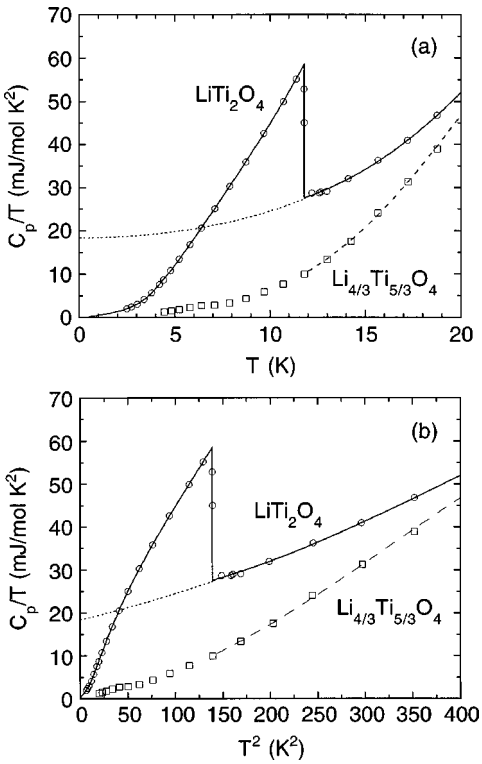

FIG. 2. Expanded plots below 20 K of the molar specific heat divided by temperature C_p/T vs temperature T of $LiTi_2O_4$ and $Li_{4/3}Ti_{5/3}O_4$ from Fig. 1. The solid curves are polynomical fits to the data for $LiTi_2O_4$, whereas the dotted curve is the inferred normal state behavior below $T_c=11.8$ K. The dashed curve is a polynomial fit to the data for $Li_{4/3}Ti_{5/3}O_4$ above 12 K.

contribution $C^{lat}(T)$ to $C_p(T)$ of LiV_2O_4. At low temperatures, the $C_p(T)$ of a conventional nonmagnetic, nonsuperconducting material is[29]

$$C_p(T)=A_1T+A_3T^3+A_5T^5+A_7T^7+\cdots, \qquad (3)$$

where $\gamma\equiv A_1$ and $\beta\equiv A_3$. From Eqs. (2), the first term in Eq. (3) is $C_e(T)$, the second corresponds to the ideal Debye lattice contribution $C^{lat}(T\rightarrow 0)$, and the following terms represent dispersion in the lattice properties.[30] The zero-temperature Debye temperature θ_0 is given by[29] $\theta_0=(1.944\times 10^6 r/\beta)^{1/3}$, where r is the number of atoms per formula unit ($r=7$ here) and β is in units of mJ/mol K^4. Equation (3) suggests the commonly used plot of C_p/T versus T^2 to obtain the parameters γ and β. Unfortunately, the very small heat capacity of the small $Li_{4/3}Ti_{5/3}O_4$ sample and the occurrence of the superconducting transition in $LiTi_2O_4$ at 11.8 K complicate the use of this relation to determine $C^{lat}(T)$ for these presumably similar materials below ≈ 12 K.

The $C_p(T)/T$ of $LiTi_2O_4$ below 20 K is plotted versus T and T^2 in Figs. 2(a) and 2(b), respectively. The superconducting transition at $T_c=11.8$ K is seen to be pronounced and very sharp ($\Delta T_c \lesssim 0.2$ K). The dotted line extrapolation of the normal state ($T>11.8$ K) data to $T=0$ shown in Figs. 1(b) and 2 uses Eq. (3), equality of the superconducting and normal state entropy at T_c, $S(11.8\ \text{K})=241(1)$ mJ/mol K, and continuity considerations with $C_p(T)/T$ above T_c, from which we also obtain estimates of γ and β. Although we cannot rule out a T dependence of γ, we assume here that γ is independent of T. While γ [$=17.9(2)$ mJ/mol K^2] appears to be quite insensitive to addenda uncertainties, θ_0 [$=700(20)$ K] is less well defined. Our value for γ is slightly smaller than the values of 20–22 mJ/mol K^2 reported earlier for $LiTi_2O_4$,[20,28] as shown in Table II. From the measured superconducting state $C_p(T_c)=684(2)$ mJ/mol K and normal state $C_p(T_c)=315(1)$ mJ/mol K, the discontinuity in C_p at T_c is given by $\Delta C_p/T_c=31.3(3)$ mJ/mol K^2, yielding $\Delta C_p/\gamma T_c=1.75(3)$ which is slightly larger than previous estimates in Table II. According to Eqs. (2), the lattice specific heat of $LiTi_2O_4$ above T_c is given by $C^{lat}(T)=C_p(T)-\gamma T$.

The $C^{lat}(T)$ derived for $LiTi_2O_4$ below 12 K is consistent within experimental uncertainties with the measured $C^{lat}(T)$ of $Li_{4/3}Ti_{5/3}O_4$ in the same temperature range after accounting for the formula weight difference. The low-T $C_p(T)/T=C^{lat}(T)/T$ for $Li_{4/3}Ti_{5/3}O_4$ is plotted in Fig. 2. The $\theta_0=725(20)$ K found for $Li_{4/3}Ti_{5/3}O_4$ is slightly larger than that for $LiTi_2O_4$, as expected. A polynomial fit to the $C_p(T)$

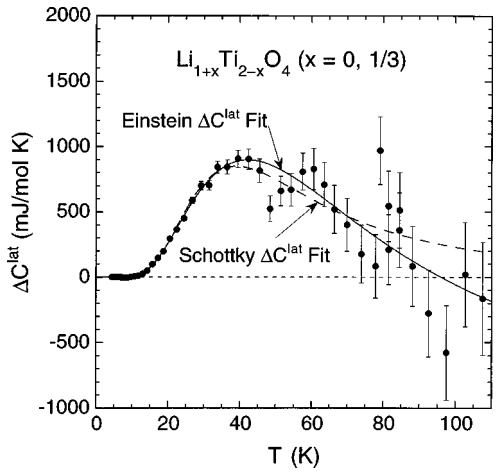

FIG. 3. The difference $\Delta C^{\rm lat}$ between the lattice specific heats of $Li_{4/3}Ti_{5/3}O_4$ and $LiTi_2O_4$ vs temperature T. The solid curve is a fit to the data by the difference between two Einstein specific heats in Eq. (4), whereas the dashed curve is the Schottky specific heat of a two-level system in Eq. (5). The error bars represent $\pm 1\%$ of the measured $C_{\rm p}(T)$ for $Li_{4/3}Ti_{5/3}O_4$.

of $Li_{4/3}Ti_{5/3}O_4$ above 12 K is shown by the dashed curves in Fig. 2. The uncertainties in the data and analyses for the Ti spinels have little effect on the analyses of $C_{\rm p}(T)$ for LiV_2O_4 in the following Sec. III C, since as Fig. 1 suggests, $C^{\rm lat}(T)$ for LiV_2O_4 is small compared to $C_{\rm e}(T)$ of this compound at low temperatures.

To quantify the difference above $\sim$12 K between the $C^{\rm lat}(T)$ of $LiTi_2O_4$ and $Li_{4/3}Ti_{5/3}O_4$ noted above in Sec. III A, in Fig. 3 is plotted the difference $\Delta C^{\rm lat}(T)$ between the measured $C_{\rm p}(T)$ of $Li_{4/3}Ti_{5/3}O_4$ and $C^{\rm lat}(T)$ of $LiTi_2O_4$. The shape of $\Delta C^{\rm lat}(T)$ in Fig. 3 below ~ 30 *K* is similar to that of an Einstein specific heat, but such a specific heat saturates to the Dulong-Petit limit at high T and does not decrease with T as the data do above 40 K. These observations suggest that intermediate-energy phonon modes in $LiTi_2O_4$ at some energy $k_{\rm B}T_{\rm E2}$ split in $Li_{4/3}Ti_{5/3}O_4$ into higher ($k_{\rm B}T_{\rm E3}$) and lower ($k_{\rm B}T_{\rm E1}$) energy modes, resulting from the Li-Ti atomic disorder on the octahedral sites in $Li_{4/3}Ti_{5/3}O_4$ and/or from the difference in the metallic character of the two compounds. Following this interpretation, we model the data in Fig. 3 as the difference $\Delta C^{\rm lat}_{\rm Einstein}$ between the Einstein heat capacities of two Einstein modes with Einstein temperatures of $T_{\rm E1}$ and $T_{\rm E2}$ (neglecting the modes at high energy $k_{\rm B}T_{\rm E3}$), given by[29]

$$\Delta C^{\rm lat}_{\rm Einstein}=3rR\left[\frac{x_1(T_{\rm E1}/2T)^2}{\sinh^2(T_{\rm E1}/2T)}-\frac{x_2(T_{\rm E2}/2T)^2}{\sinh^2(T_{\rm E2}/2T)}\right], \quad (4)$$

where R is the molar gas constant, $r=7$ atoms/formula unit, and x_1 and x_2 are the fractions of the total number of phonon modes shifted to $T_{\rm E1}$ and away from $T_{\rm E2}$, respectively. A reasonable fit of the data by Eq. (4) was obtained with the parameters $x_1=0.012$, $T_{\rm E1}=110$ K, $x_2=0.018$, and $T_{\rm E2}=240$ K; the fit is shown as the solid curve in Fig. 3. The model then predicts that a fraction $(x_2-x_1)/x_2\sim 0.3$ of the modes removed at energy $k_{\rm B}T_{\rm E2}$ are moved to an energy $k_{\rm B}T_{\rm E3}\gg k_{\rm B}T_{\rm E2}$.

An alternative parametrization of the experimental $\Delta C^{\rm lat}(T)$ data can be given in terms of the specific heat of a two-level system, described by the Schottky function[29]

$$\Delta C^{\rm lat}_{\rm Schottky}=xrR\left(\frac{g_0}{g_1}\right)\left(\frac{\delta}{T}\right)^2\frac{e^{\delta/T}}{[1+(g_0/g_1)e^{\delta/T}]^2}, \quad (5)$$

where x is the atomic fraction of two-level sites, g_0 and g_1 are, respectively, the degeneracies of the ground and excited levels, and δ is the energy level splitting in temperature units. Fitting Eq. (5) to the data in Fig. 3, we find $g_1/g_0=4$, $x=0.012$ and $\delta=117$ K. The fit is shown as the dashed curve in Fig. 3. The accuracy of our $\Delta C^{\rm lat}(T)$ data is not sufficient to discriminate between the applicability of the Einstein and Schottky descriptions.

C. LiV_2O_4

Specific heat $C_{\rm p}(T)$ data were obtained for samples from four batches of LiV_2O_4. Our first experiment was carried out on sample 2 (run 1) with mass 5 g. The $C_{\rm p}(T)$ was found to be so large at low T (the first indication of heavy-fermion behavior in this compound from these measurements) that the large thermal diffusivity limited our measurements to the 2.23–7.94 K temperature range. A smaller piece of sample 2 (0.48 g) was then measured (run 2) from 1.16 to 78.1 K. Data for samples from two additional batches (sample 3 of mass 0.63 g, 1.17–29.3 K, and sample 4A of mass 0.49 g, 1.16–39.5 K) were also obtained. Subsequent to the theoretical modeling of the data for sample 3 described below in Sec. V, we obtained a complete data set from 1.14 to 108 K for sample 6 with mass 1.1 g from a fourth batch. A power series fit to the $C_{\rm p}(T)$ data for sample 6 is shown as solid curves in Fig. 1.

We have seen above that $C^{\rm lat}(T)$ of $LiTi_2O_4$ is significantly different from that of $Li_{4/3}Ti_{5/3}O_4$. Since LiV_2O_4 is a metallic normal-spinel compound with cation occupancies $Li[V_2]O_4$ as in $Li[Ti_2]O_4$, and since the formula weight of metallic $LiTi_2O_4$ is much closer to that of LiV_2O_4 than is that of the insulator $Li_{4/3}Ti_{5/3}O_4$, we expect that the lattice dynamics and $C^{\rm lat}(T)$ of LiV_2O_4 are much better approximated by those of $LiTi_2O_4$ than of $Li_{4/3}Ti_{5/3}O_4$. Additionally, more precise and accurate $C_{\rm p}(T)$ data were obtained for $LiTi_2O_4$ as compared to $Li_{4/3}Ti_{5/3}O_4$ because of the factor of 3 larger mass of the former compound measured than of the latter. Therefore, we will assume in the following that the $C^{\rm lat}(T)$ of LiV_2O_4 for 0–108 K is identical with that given above for $LiTi_2O_4$. We do not attempt to correct for the influence of the small formula weight difference of 3.5% between these two compounds on $C^{\rm lat}(T)$; this difference would only be expected to shift the Debye temperature by $\lesssim 1.8\%$, which is on the order of the accuracy of the high temperature $C_{\rm p}(T)$ data. The $C_{\rm e}(T)$ of LiV_2O_4 is then obtained using Eq. (2a).

The $C_{\rm e}(T)$ data for samples 2 (run 2) and 6 of LiV_2O_4, obtained using Eqs. (2), are shown up to 108 K in plots of $C_{\rm e}(T)$ and $C_{\rm e}(T)/T$ vs T in Figs. 4(a) and 4(b), respectively. An expanded plot of $C_{\rm e}(T)$ below 9 K for LiV_2O_4 is shown in Fig. 5(a), where data for sample 2 (run 1) and sample 3 are also included. The data for samples 2 and 3 are seen to be in agreement to within about 1%. However, there is a small

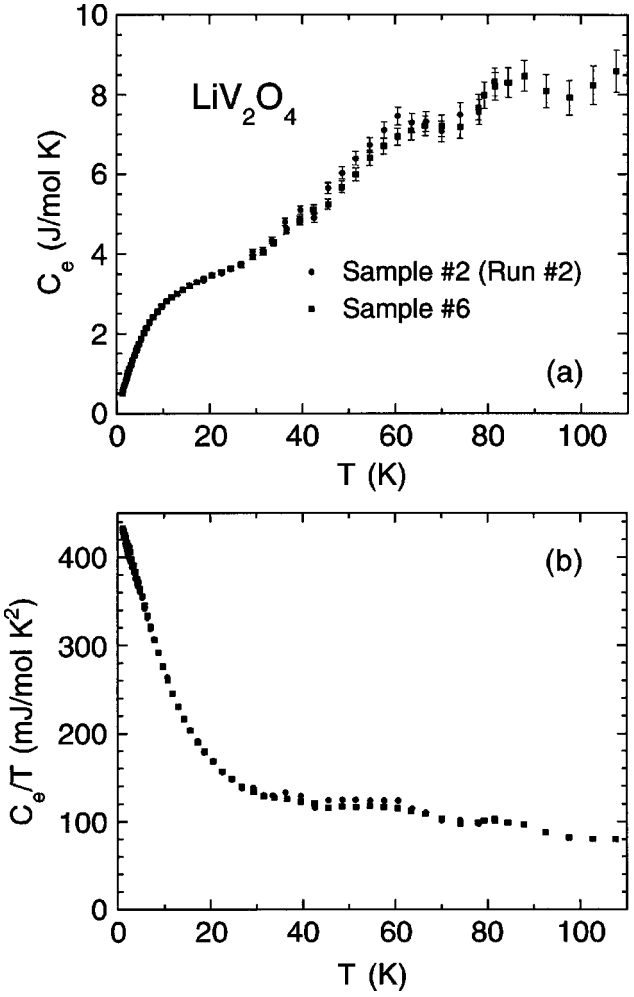

FIG. 4. Electronic specific heat C_e (a) and C_e/T (b) vs. temperature T for LiV_2O_4 samples 2 (run 2) and 6. The error bars in (a) represent $\pm 1\%$ of the measured $C_p(T)$ for LiV_2O_4.

positive curvature in the data for sample 2 below ~ 3 K, contrary to the small negative curvature for sample 3. This difference is interpreted to reflect the influence of the larger magnetic defect concentration present in sample 2 as compared with that in sample 3; see Table I.[5] Therefore, we believe that the $C_e(T)$ data for sample 3 more closely reflect

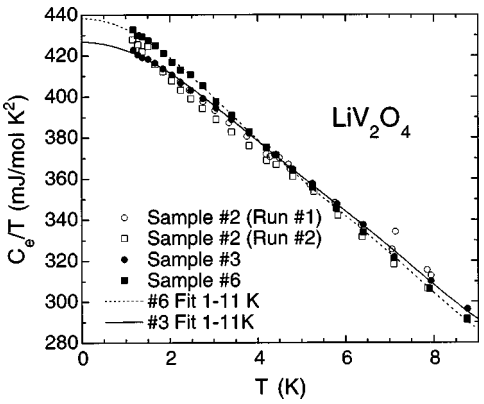

FIG. 5. Expanded plot below 9 K of the C_e/T vs T data for LiV_2O_4 samples 2, 3, and 6. The solid and dashed curves are polynomial fits to the 1.1–10 K data for samples 3 and 6, respectively.

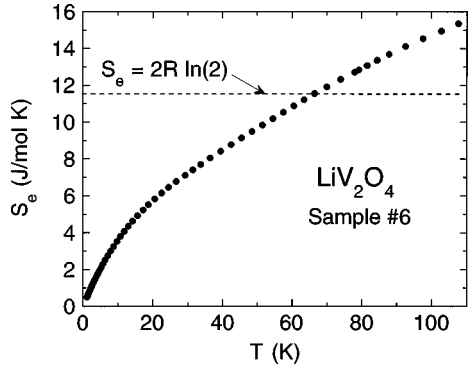

FIG. 6. Electronic entropy S_e of LiV_2O_4 sample 6 vs temperature T (●), obtained by integrating the C_e/T data for sample 6 in Fig. 4(b) with T.

the intrinsic behavior of defect-free LiV_2O_4 compared to the data for sample 2 and all fits to $C_e(T)$ of LiV_2O_4 below 30 K by theoretical models to be presented in Sec. V below are therefore done using the data for sample 3. As seen in Fig. 5(a), the $C_e(T)$ data for sample 6 lie somewhat higher than the data for the other samples below about 4 K but are comparable with those for the other samples at higher temperatures. This difference is also reflected in the magnetic susceptibilities $\chi(T)$,[5] where $\chi(T)$ for sample 6 is found to be slightly larger than those of other samples.

To obtain extrapolations of the electronic specific heat to $T=0$, the $C_e(T)/T$ data in Fig. 5 from 1 to 10 K for samples 3 and 6 were fitted by the polynomial

$$\frac{C_e(T)}{T} = \gamma(0) + \sum_{n=1}^{5} C_{2n} T^{2n}, \tag{6}$$

yielding

$$\gamma(0) = 426.7(6)\ \text{mJ/mol K}^2 \quad \text{(sample 3)}, \tag{7a}$$

$$\gamma(0) = 438.3(5)\ \text{mJ/mol K}^2 \quad \text{(sample 6)}. \tag{7b}$$

The fits for samples 3 and 6 are, respectively, shown by solid and dashed curves in Fig. 5. The $\gamma(0)$ values are an order of magnitude or more larger than typically obtained for

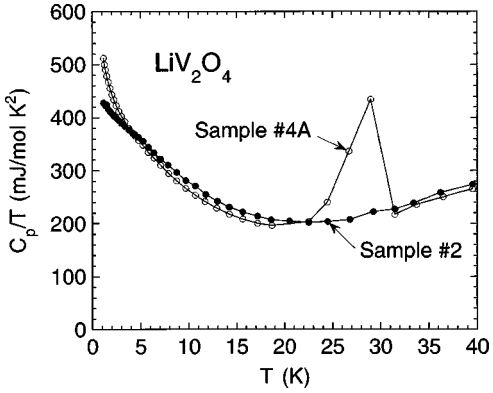

FIG. 7. Measured specific heat divided by temperature C_p/T vs. temperature T for LiV_2O_4 sample 4A; corresponding data for sample 2 from Fig. 1 are shown for comparison. The lines are guides to the eye.

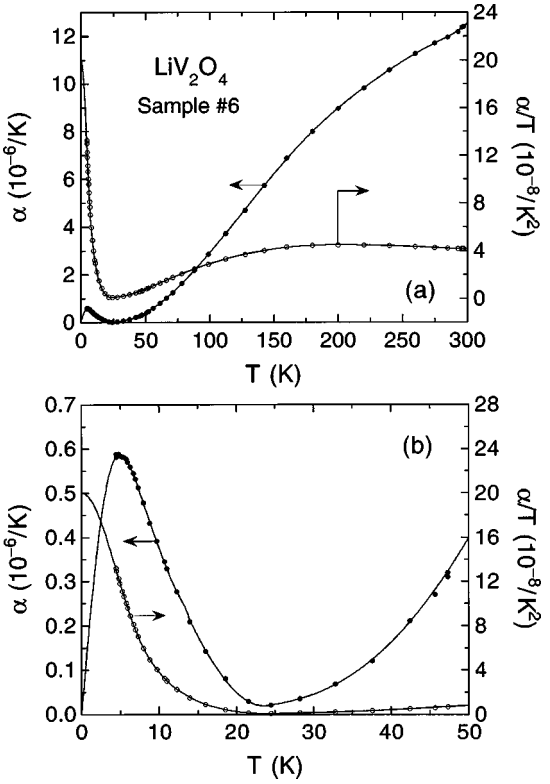

FIG. 8. Linear thermal expansion coefficient α (left-hand scales) and α/T (right-hand scales) versus temperature T for LiV_2O_4 sample 6 from 4.4 to 297 K (a) and 4.4 to 50 K (b). The solid curves are the fit to the $\alpha(T)$ data by a polynomial.

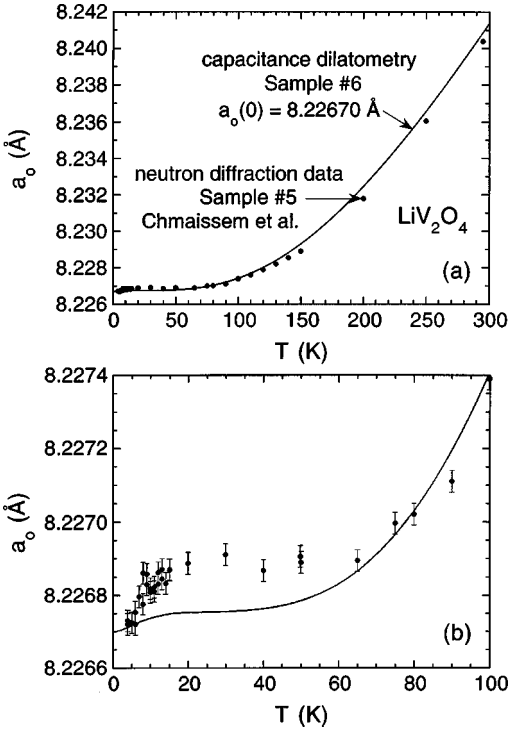

FIG. 9. Lattice parameter a_0 vs temperature T from 4 to 297 K (a) and an expanded plot from 4 to 100 K (b) for LiV_2O_4. The solid circles are the neutron diffraction measurements of sample 5 by Chmaissem and co-workers (Refs. 4 and 8). The solid curve is the linear thermal dilation obtained from our capacitance dilatometer measurements of sample 6, assuming $a_0(0) = 8.22670$ Å.

transition-metal compounds, and are about 23 times larger than found above for $LiTi_2O_4$.

The T-dependent electronic entropy $S_e(T)$ of LiV_2O_4 was obtained by integrating the $C_e(T)/T$ data for sample 6 in Fig. 4(b) with T; the extrapolation of the $C_e(T)/T$ vs T fit for sample 6 in Fig. 5 from $T = 1.16$ K to $T = 0$ yields an additional entropy of $S_e(1.16\ \text{K}) = 0.505$ J/mol K. The total $S_e(T)$ is shown up to 108 K in Fig. 6; these data are nearly identical with those of sample 2 (run 2) up to the maximum measurement temperature of 78 K for that sample (not shown). The electronic entropy at the higher temperatures is large. For example, if LiV_2O_4 were to be considered to be a strictly localized moment system with one spin $S = 1/2$ per V atom, then the maximum electronic (spin) entropy would be $2R\ln(2)$, which is already reached at about 65 K as shown by comparison of the data with the horizontal dashed line in Fig. 6.

Our $C_p(T)$ data for one sample (sample 4A) of LiV_2O_4 were anomalous. These are shown in Fig. 7 along with those of sample 2 (run 2) for comparison. Contrary to the $C_p(T)/T$ data for sample 2, the data for sample 4A show a strong upturn below ~ 5 K and a peak at about 29 K. We have previously associated the first type of effect with significant (~ 1 mol %) concentrations of paramagnetic defects.[4] Indeed, Table I shows that this sample has by far the highest magnetic impurity concentration of all the samples we studied in detail. The anomalous peak at 29 K might be inferred to be due to small amounts of impurity phases (see Table I). However, the excess entropy ΔS under the peak is rather large, $\Delta S \sim 0.9$ J/mol K $\approx 0.16R\ln(2)$. We also note that the height of the anomaly above ''background'' is at least an order of magnitude larger than would be anticipated due to a few percent of V_4O_7 or V_5O_9 impurity phases which order antiferromagnetically with Néel temperatures of 33.3 and 28.8 K, respectively.[31] It is possible that the 29 K anomaly is intrinsic to the spinel phase in this particular sample; in such a case Li-V antisite disorder and/or other types of crystalline defects would evidently be involved. As seen in Table I, this sample has by far the largest room temperature lattice parameter of all the samples listed, which may be a reflection of a slightly different stoichiometry and/or defect distribution or concentration from the other samples. The intrinsic $\chi(T)$ derived for the spinel phase in this sample is also anomalous.[5] Although these $C_p(T)$ data for sample 4A will not be discussed further in this paper, the origin of the anomaly at 29 K deserves further investigation.

IV. THERMAL EXPANSION MEASUREMENTS

The linear thermal expansion coefficient $\alpha(T)$ of LiV_2O_4 sample 6 was measured between 4.4 and 297 K. Figure 8(a) shows $\alpha(T)$ and $\alpha(T)/T$ over this T range, and Fig. 8(b) shows expanded plots below 50 K. At 297 K, $\alpha = 12.4 \times 10^{-6}$ K^{-1}, which may be compared with the value $\alpha \approx 15.6 \times 10^{-6}$ K^{-1} obtained for $LiTi_2O_4$ between 293 and 1073 K from x-ray diffraction measurements.[32] Upon cooling from 297 K to about 25 K, α of LiV_2O_4 decreases as is typical of conventional metals.[30] However, $\alpha(T)$ nearly becomes negative with decreasing T at about 23 K. This trend is preempted upon further cooling below ~ 20 K, where both

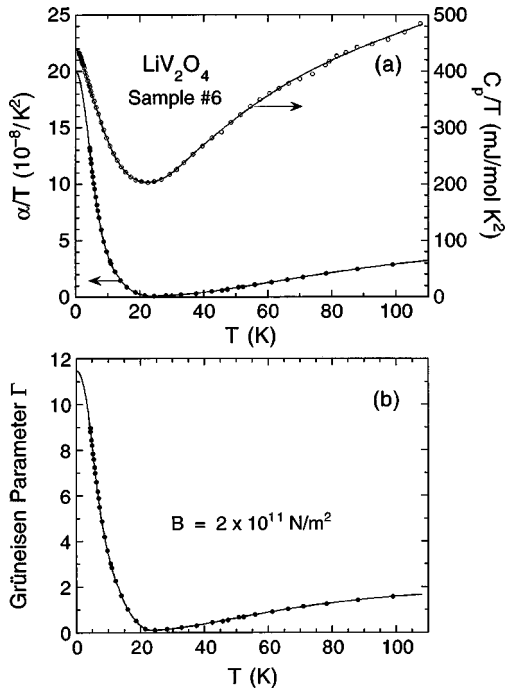

FIG. 10. (a) Comparison of the linear thermal expansion coefficient divided by temperature $\alpha(T)/T$ (left-hand scale) with the measured specific heat $C_p(T)/T$ (right-hand scale) for LiV_2O_4 sample 6. (b) Grüneisen parameter Γ vs T, computed using Eq. (8) and the assumed value of the bulk modulus B given in the figure.

$\alpha(T)$ and $\alpha(T)/T$ exhibit strong increases. The strong increase in $\alpha(T)$ below 20 K was first observed by Chmaissem *et al.*[8] from high-resolution neutron diffraction data, which motivated the present $\alpha(T)$ measurements. We fitted our $\alpha(T)$ data by a polynomial in T over three contiguous temperature ranges and obtained the fit shown as the solid curves in Figs. 8. From the fit, we obtain $\lim_{T\to 0}\alpha(T)/T = 2.00\times10^{-7}\,\mathrm{K}^{-2}$.

Shown as the solid curve in Fig. 9(a) is the linear thermal dilation expressed in terms of the lattice parameter $a_0(T) = a_0(0)[1+\int_0^T \alpha(T)\,dT]$, where we have used our polynomial fit to the $\alpha(T)$ data to compute $a_0(T)$ and have set $a_0(0) = 8.22670$ Å. The $a_0(T)$ determined from the neutron diffraction measurements by Chmaissem *et al.*[8] for a different sample (sample 5) are plotted as the solid circles in Fig. 9. The two data sets are in overall agreement, and both indicate a strong decrease in $a_0(T)$ with decreasing T below 20 K. There are differences in detail between the two measurements at the lower temperatures as illustrated below 100 K in Fig. 9(b), suggesting a possible sample dependence.

Our measurement of $\alpha(T)/T$ for sample 6 is compared with the measured $C_p(T)/T$ for the same sample in Fig. 10(a), where the temperature dependences of these two quantities are seen to be similar. We infer that the strong increase in $\alpha(T)/T$ with decreasing T below $\sim$20 K is an electronic effect associated with the crossover to heavy-fermion behavior. For most materials, the volume thermal expansivity $\beta = 3\alpha$ and C_p are related through the dimensionless Grüneisen parameter Γ, with[30]

$$\beta = \frac{\Gamma C_p}{B_s V_M}, \tag{8}$$

TABLE III. Parameters for LiV_2O_4. Abbreviations: formula weight FW, lattice parameter a_0,[4,8] (formula units/unit cell) Z, theoretical mass density ρ^{calc}, molar volume V_M, itinerant electron concentration N_e/V, Fermi wave vector $k_F = (3\pi^2 N_e/V)^{1/3}$, effective mass m^* (free electron mass m_e), Fermi velocity $v_F = \hbar k_F/m^*$, Fermi energy $E_F = \hbar^2 k_F^2/2m^*$; Fermi temperature $T_F = E_F/k_B$, and mass-enhanced density of states at E_F for both spin directions, $\mathcal{D}^*(E_F) = 3N_e/(2E_F) = m^* k_F V/(\pi^2\hbar^2)$.

Property	Value
FW	172.82 g/mol
a_0(12 K)	8.2269 Å
Z	8
ρ^{calc}(12 K)	4.123 g/cm^3
V_M	41.92 cm^3/mol
N_e/V	4.310×10^{22} cm^{-3}
k_F	1.0847 Å^{-1}
m^*/m_e	180.5
v_F	6.96×10^5 cm/s
E_F	24.83 meV
T_F	288.1 K
$\mathcal{D}^*(E_F)$	90.6 states/eV(V atom)

where B_s is the adiabatic bulk modulus and V_M is the molar volume. In this model, $\Gamma = -d\ln\Phi/d\ln V$ where $\Phi(V)$ is a characteristic energy of the system. If independent contributions to C_p can be identified, as assumed in Eq. (2a), a relation similar to Eq. (2a) exists for the thermal expansivity, with an independent Γ for each contribution:

$$\beta = \beta_e + \beta^{lat} = \frac{\Gamma_e C_e + \Gamma^{lat} C_p^{lat}}{B_s V_M}, \tag{9}$$

where C_e is understood to refer to measurements under constant pressure. For a metal, $\Gamma_e = d\ln\mathcal{D}^*(E_F)/d\ln V = d\ln\gamma(0)/d\ln V$, and $\Gamma^{lat} = -d\ln\theta_0/d\ln V$. Here $\mathcal{D}^*(E_F)$ is the mass-enhanced quasiparticle density of states at the Fermi energy and the volume dependence of the electron-phonon interaction is neglected. Thus Γ_e is a direct measure of the volume dependence of $\mathcal{D}^*(E_F)$. For a free electron gas, $\Gamma_e = 2/3$. For most real metals $\Gamma_e = \pm 3(2)$, e.g., $\Gamma_e = 0.92$ (Cu), 1.6 (Au), 1.6 (V), -4.4 (Sr), -0.2 (Ba), and 2.22 (Pd).[30]

We have computed $\Gamma(T)$ for LiV_2O_4 from Eq. (8) using the polynomial fit to our C_p data for sample 6 and using the experimental $\alpha(T)$ data in Fig. 8 for this sample. The molar volume of LiV_2O_4 at low temperatures is given in Table III. The bulk modulus is assumed to be $B = 200(40)$ GPa, which is the range found[33] for the similar compounds Fe_2O_3, Fe_3O_4, $FeTiO_3$, MgO, TiO_2 (rutile), the spinel prototype $MgAl_2O_4$,[34] and $MgTi_2O_5$.[35] The Γ obtained by substituting these values into Eq. (8) is plotted versus temperature as the solid circles in Fig. 10(b). Interpolation and extrapolation of $\Gamma(T)$ is obtained from the polynomial fit to the $\alpha(T)$ data, shown by the solid curve in Fig. 10(b). From Fig. 10(b), $\Gamma \approx 1.7$ at 108 K and decreases slowly with decreasing T, reaching a minimum of about 0.1 at 23 K. With a further decrease in T, Γ shows a dramatic increase and we obtain an extrapolated $\Gamma(0) \approx 11.4$. A plot of Γ vs T^2 obtained from our experimental data points is linear for $T^2 < 30$ K^2, and

extrapolates to 11.50 at $T=0$, to be compared with 11.45 as calculated from the smooth fitted relations for $\alpha(T)$ and $C_p(T)$; this justifies the (long) extrapolation of $\alpha(T)$ to $T=0$. An accurate determination of the magnitude of Γ must await the results of bulk modulus measurements on LiV_2O_4. Our estimated $\Gamma(0)\equiv\Gamma_e(0)$ is intermediate between those of conventional nonmagnetic metals and those of *f*-electron heavy-fermion compounds such as UPt_3 ($\Gamma_e=71$), UBe_{13} (34), and $CeCu_6$ (57) with $\gamma(0)=0.43$, 0.78, and 1.67 J/mol K^2, respectively.[36]

From the expression[29] relating C_p to the specific heat at constant volume C_v, and using our $\alpha(T)$ data and the estimate for B above, $C_v(T)$ of LiV_2O_4 can be considered identical with our measured $C_p(T)$ to within both the precision and accuracy of our measurements up to 108 K.

V. THEORETICAL MODELING: ELECTRONIC SPECIFIC HEAT OF LiV_2O_4

A. Single-band spin $S=1/2$ Fermi liquid

As mentioned in Sec. I, the high-temperature $\chi(T)$ of LiV_2O_4 indicated a vanadium local moment with spin $S=1/2$ and $g\sim2$. In the low-temperature Fermi liquid regime, for a Fermi liquid consisting of a single parabolic band of quasiparticles with $S=1/2$ and N_e conduction electrons per unit volume V,[37–40] the Fermi wave vector k_F of LiV_2O_4 assuming $N_e=1.5$ conduction electrons/V atom is given in Table III. In terms of the mass-enhanced density of states at the Fermi energy E_F for both spin directions $\mathcal{D}^*(E_F)$, the $\gamma(0)$ (neglecting electron-phonon interactions) and $\chi(0)$ are given by

$$\gamma(0)=\frac{\pi^2 k_B^2}{3}\mathcal{D}^*(E_F), \tag{10a}$$

$$\chi(0)=\frac{g^2\mu_B^2}{4}\frac{\mathcal{D}^*(E_F)}{1+F_0^a}, \tag{10b}$$

where F_0^a is a Landau Fermi liquid parameter and $1/(1+F_0^a)=1-A_0^a$ is the Stoner enhancement factor. The Fermi liquid scattering amplitudes $A_l^{a,s}$ are related to the Landau parameters $F_l^{a,s}$ by $A_l^{a,s}=F_l^{a,s}/[1+F_l^{a,s}/(2l+1)]$. The superscripts ''a'' and ''s'' refer to spin-asymmetric and spin-symmetric interactions, respectively. Using Eq. (10a) and the k_F value in Table III, the experimental value of $\gamma(0)$ for LiV_2O_4 in Eq. (7a) yields the effective mass m^*, Fermi velocity v_F, E_F, Fermi temperature T_F, and $\mathcal{D}^*(E_F)$ for LiV_2O_4 given in Table III. From Eqs. (1) and (10), the Wilson ratio[2] R_W is expressed as

$$R_W=\frac{1}{1+F_0^a}=1-A_0^a. \tag{11}$$

Substituting the experimental $\chi(0.4\text{–}2\ \mathrm{K})=0.0100(2)$ cm^3/mol (Ref. 4) and $\gamma(0)$ in Eq. (7a) for LiV_2O_4 into Eq. (1) assuming $g=2$ yields

$$R_W=1.71(4). \tag{12}$$

This R_W value is in the range of those found for many conventional as well as *f*-electron HF and IV compounds.[1] The R_W value in Eq. (12) yields from Eq. (11)

$$F_0^a=-0.42,\quad A_0^a=-0.71. \tag{13}$$

In Fermi liquid theory, a temperature dependence is often computed for C_e at low temperatures having the form[38–40]

$$C_e(T)=\gamma(0)T+\delta T^3\ln\left(\frac{T}{T_0}\right)+\mathcal{O}(T^3), \tag{14}$$

where $\gamma(0)$ is given by Eq. (10a) and T_0 is a scaling or cutoff temperature. Engelbrecht and Bedell[41] considered a model of a single-band Fermi liquid with the microscopic constraint of a local (momentum-independent) self-energy, where the interactions are mediated by the quasiparticles themselves (in the small-momentum-transfer limit). They find that only *s*-wave ($l=0$) Fermi liquid parameters can be nonzero and that the δ coefficient in Eq. (14) is

$$\delta_{EB}=\frac{3\pi^2}{5}\frac{\gamma(0)}{T_F^2}(A_0^a)^2\left(1-\frac{\pi^2}{24}A_0^a\right), \tag{15}$$

where $|A_0^{a,s}|\leq1$ and $-\frac{1}{2}\leq F_0^{a,s}<\infty$. Within their model, neither ferromagnetism nor phase separation can occur. For $F_0^a<0$, the only potential instability is towards antiferromagnetism and/or a metal-insulator transition; in this case they find $1\leq R_W\leq2$. For $F_0^a>0$, a BCS superconducting state is possible and $R_W<1$. The value of F_0^a for LiV_2O_4 in Eq. (13) is within the former range of this theory.

Auerbach and Levin[42] and Millis and Lee[43,44] formulated a Fermi liquid theory of heavy-electron compounds at low temperatures on the basis of a microscopic Kondo lattice model. The large enhancement of m^* arises from the spin entropy of the electrons on the magnetic-ion sites (i.e., spin fluctuations).[43] The Wilson ratio is $R_W\sim1.5$ and a $T^3\ln T$ contribution to $C_e(T)$ is found. The origin of this latter term is not ferromagnetic spin fluctuations (''paramagnons''),[42] but is rather electron density fluctuations and the screened long-range Coulomb interaction.[43] The coefficient δ_M of the $T^3\ln T$ term found by Millis[43] is $\delta_M=\pi^2k_B^4V(1-\pi^2/12)/5(\hbar v_F)^3$, which may be rewritten as

$$\delta_M=\frac{3\pi^2\gamma(0)}{20T_F^2}\left(1-\frac{\pi^2}{12}\right). \tag{16}$$

Using the values $\gamma(0)=427$ mJ/mol K^2 [Eq. (7a)], $T_F=288$ K (Table III) and A_0^a in Eq. (13), Eqs. (15) and (16), respectively, predict

$$\delta_{EB}=0.0199\frac{\mathrm{mJ}}{\mathrm{mol\,K^4}},\quad \delta_M=0.00135\frac{\mathrm{mJ}}{\mathrm{mol\,K^4}}. \tag{17}$$

We have fitted our low-temperature $C_e(T)/T$ data for LiV_2O_4 sample 3 by the expression

$$\gamma(T)\equiv\frac{C_e(T)}{T}=\gamma(0)+\delta T^2\ln\left(\frac{T}{T_0}\right)+\varepsilon T^3, \tag{18}$$

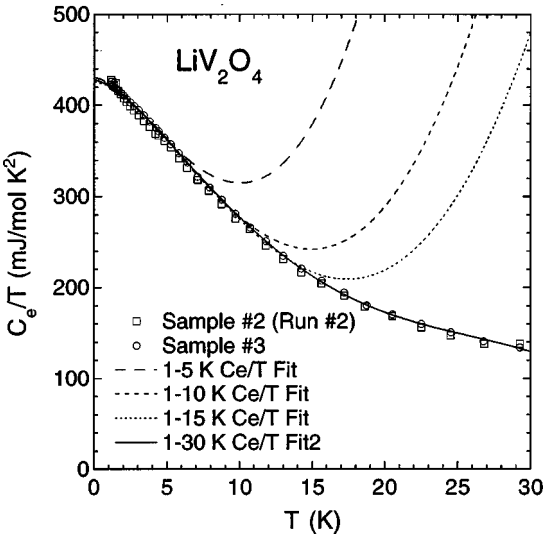

FIG. 11. Electronic specific heat C_e divided by temperature T for LiV_2O_4 samples 2 (run 2) and 3 vs T. The dashed curves are fits to the 1–5 K, 1–10 K, and 1–15 K data for sample 3 by the spin-fluctuation Fermi liquid model, Eq. (18) with $\varepsilon=0$, whereas the solid curve is a 1–30 K fit assuming $\varepsilon\neq 0$.

initially with $\varepsilon=0$. The fit parameters $\gamma(0)$, δ, and T_0 were found to depend on the fitting temperature range above 1 K chosen, and are sensitive to the precision of the data. The parameters obtained for 1–3 K and 1–5 K fits were nearly the same, but changed when the upper limit to the fitting range was increased to 10 and 15 K. The fits for the 1–5 K, 1–10 K, and 1–15 K fitting ranges are shown in Fig. 11, along with the $C_e(T)/T$ data for sample 2 (run 2). As a check on the fitting parameters, we have also fitted the $C_e(T)/T$ data for sample 3 by Eq. (18) with ε as an additional fitting parameter. The fit for the 1–30 K range is plotted as the solid curve in Fig. 11. The fits for the smaller T ranges with $\varepsilon=0$ and for the larger ranges with $\varepsilon\neq 0$ should give the most reliable parameters. We infer from the fit parameters for all ranges that the most likely values of the parameters and their error bars are

$$\gamma(0)=428(2)\,\frac{\text{mJ}}{\text{mol K}^2},\qquad \delta=1.9(3)\frac{\text{mJ}}{\text{mol K}^4}. \tag{19}$$

The parameters in Eq. (19) are very similar to those obtained using the same type of fit to $C_p(T)/T$ data for the heavy-fermion superconductor UPt_3 with $T_c=0.54$ K,[45] for which $\gamma(0)=429$–450 mJ/mol K^2 and $\delta=1.99$ mJ/mol K^4.[45,46] Our T_F and m^*/m_e values for LiV_2O_4 (288 K and 181, Table III) are also, respectively, very similar to those of UPt_3 (289 K and 178).[39]

The experimental δ value in Eq. (19) is a factor of $\sim 10^2$ larger than δ_{EB} and $\sim 10^3$ larger than δ_M predicted in Eq. (17). A similar large $[\mathcal{O}(10^2$–$10^3)]$ discrepancy was found by Millis for the δ coefficient for UPt_3.[43] As explained by Millis,[43] the large discrepancy between his theory and experiment may arise because the calculations are for a single parabolic band, an assumption which may not be applicable to the real materials. However, he viewed the most likely reason to be that his calculations omit some effect important to the thermodynamics such as antiferromagnetic spin fluctuations.[43] In this context, it is possible that the magnitude of δ predicted by one of the above two theories is correct, but that terms higher order in T not calculated by the theory are present which mask the $T^3 \ln T$ contribution over the temperature ranges of the fits;[47] in this case the large experimental δ value would be an artifact of force fitting the data by Eq. (18). Indeed, we found that the fits were unstable, i.e., depended on the temperature range fitted (cf. Fig. 11). In addition, the applicability of the theory of Millis[43] to LiV_2O_4 is cast into doubt by the prediction that the Knight shift at a nucleus of an atom within the conduction electron sea (not a ''magnetic'' atom) ''would be of the same order of magnitude as in a normal metal, and would not show the mass enhancement found in χ.''[44] In fact, the Knight shift of the ^{7}Li nucleus in LiV_2O_4 for $T\sim 1.5$–10 K is about 0.14%,[4,6,10,11] which is about 600 times larger than the magnitude (0.00024%) found[48] at room temperature for the ^{7}Li Knight shift in $LiTi_2O_4$. Similarly, the ^{7}Li $1/T_1T$ from 1.5 to 4 K in the highest-purity LiV_2O_4 samples is about 2.25 s^{-1}K^{-1},[4,6] which is about 6000 times larger than the value of 3.7×10^{-4} s^{-1}K^{-1} found[48] at 160 K in $LiTi_2O_4$, where T_1 is the ^{7}Li nuclear spin-lattice relaxation time.

B. Quantum-disordered antiferromagnetically coupled metal

The antiferromagnetic (AF) Weiss temperature of LiV_2O_4 from $\chi(T)$ measurements is $|\theta|=30$–60 K, yet the pure system exhibits neither static AF nor spin-glass order above 0.02 K.[4,5] A possible explanation is that the ground state is disordered due to quantum fluctuations. We consider here the predictions for $C_e(T)$ of one such theory. A universal contribution to the temperature dependence of C_e of a three-dimensional (3D) metal with a control parameter r near that required for a zero-temperature AF to quantum-disordered phase transition, corresponding to dynamical exponent $z=2$, was calculated by Zülicke and Millis,[24] which modifies the Fermi liquid prediction in Eq. (14). Upon increasing T from $T=0$ in the quantum-disordered region, the system crosses over from the quantum disordered to a classical regime. The same scaling theory predicts that the low-T spin susceptibility is given by $\chi(T)=\chi(0)+AT^{3/2}$, where the constant A is not determined by the theory.[49]

Zülicke and Millis found the electronic specific heat to be given by[24]

$$\frac{C_e}{T}=\gamma_0-\frac{\alpha R N_0\sqrt{r}}{6T^*}F\left(\frac{T}{rT^*}\right), \tag{20a}$$

$$F(x)=\frac{3\sqrt{2}}{\pi^2}\int_0^\infty dy\,\frac{y^2}{\sinh^2 y}\sqrt{1+\sqrt{1+4x^2y^2}}. \tag{20b}$$

Here, γ_0 is the (nonuniversal) electronic specific heat coefficent at $T=0$ in the usual Fermi liquid theory [$\gamma(0)$ above], T^* is a characteristic temperature, and N_0 is the number of components of the bosonic order parameter which represents the ordering field: $N_0=3$, 2, 1 for Heisenberg, XY, and Ising symmetries, respectively. The number α is not determined by the scaling theory but is expected to be on the order of the number of conduction electrons per formula unit; thus for LiV_2O_4, we expect $\alpha\sim 3$. We have defined $F(x)$ such that

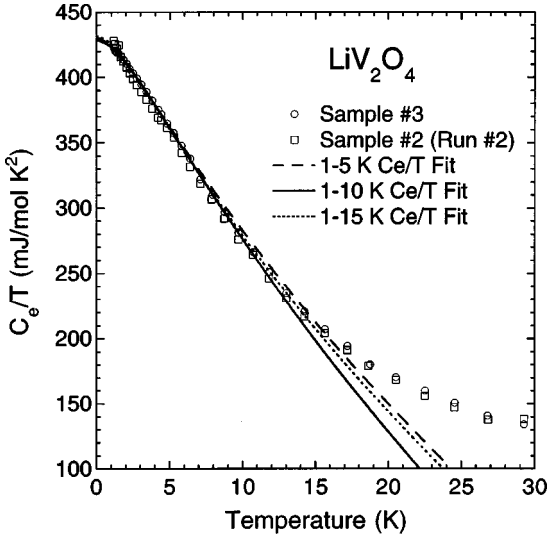

FIG. 12. Electronic specific heat divided by temperature C_e/T vs T for LiV_2O_4 samples 2 (run 2) and 3. Fits to the data for sample 3 by the theory of Zülicke and Millis (Ref. 24), Eqs. (20), are shown for the fitting ranges 1–5 K (long-dashed curve), 1–10 K (solid curve), and 1–15 K (short-dashed curve).

$F(0)=1$. The variable r is expected to be temperature dependent, but this temperature dependence cannot be evaluated without ascertaining the value of an additional parameter u in the theory from, e.g., measurements of the pressure dependence of $C_e(T)$; here, we will assume r to be a constant.[50] From Eq. (20a), the $T=0$ value of γ in the absence of quantum fluctuations is reduced by these fluctuations, and the measured $\gamma(0)$ is

$$\gamma(0)=\gamma_0-\frac{\alpha R N_0\sqrt{r}}{6T^*}. \tag{21}$$

We fitted our C_e/T vs T data for LiV_2O_4 sample 3 by Eqs. (20), assuming $N_0=3$. The fitting parameters were γ_0, α, r, and T^*; the $\gamma(0)$ value is then obtained from Eq. (21). The 1–20 K and larger ranges did not give acceptable fits. The fits for the 1–5, 1–10, and 1–15 K fitting ranges are shown in Fig. 12. From these fits, we infer the parameters and errors

$$\gamma_0=800(50)\,\frac{\text{mJ}}{\text{mol K}^2},\quad \alpha=2.65(9),\quad r=0.40(6),$$

$$T^*=18.9(4)\text{ K},\quad \gamma(0)=430(1)\text{ mJ/mol K}^2. \tag{22}$$

Within the context of this theory, quantum fluctuations reduce the observed $\gamma(0)$ by about a factor of 2 compared to the value γ_0 in the absence of these fluctuations. The value of α is close to the nominally expected value ~ 3 mentioned above. The relatively large value of r indicates that LiV_2O_4 is not very close to the quantum-critical point, and therefore predicts that long-range AF order will not be induced by small changes in external conditions (pressure) or composition. The former prediction cannot be checked yet because the required experiments under pressure have not yet been done. The latter expectation is consistent with the data available so far. Magnetic defect concentrations on the order of 1% do induce static magnetic ordering below ~ 0.8 K, but this ordering is evidently of the short-range spin-glass type.[4] Substitution of Zn for Li in $Li_{1-x}Zn_xV_2O_4$ induces spin-glass ordering for $0.2\lesssim x\lesssim 0.9$ but long-range AF ordering does not occur until $0.9\lesssim x\leqslant 1.0$.[9] Finally, two caveats regarding the fits and discussion in this section are in order. The first is that (unknown) corrections of order $(T/T^*)^2$ and r^1 to the theory of Zülicke and Millis[24] exist but have not been included in the prediction in Eqs. (20); incorporating these corrections may alter the parameters obtained from fits to experimental data.[51] The second caveat is that the theory may need modification for compounds such as LiV_2O_4 in which geometric frustration for AF ordering exists in the structure.[51]

C. Spin-1/2 Kondo model

Calculations of the impurity spin susceptibility $\chi(T)$ and/or impurity electronic contribution $C_e(T)$ to the specific heat for the $S=1/2$ Kondo model were carried out by Wilson[2] and others[52–59] using different techniques. Both $\chi(T)$ and $C_e(T)$ depend only on the scaling parameter T/T_K, where T_K is the Kondo temperature (here, we use Wilson's definition[2]). The impurity $\chi(T)$ is predicted to be Curie-Weiss-like at temperatures high compared with T_K, and to level out at a constant high value for $T\lesssim 0.1T_K$ due to the formation of a singlet ground state.

In the limit of zero temperature, one has[56]

$$\gamma(T=0)=\frac{\pi W N k_B}{6T_K}, \tag{23}$$

where N is the number of impurity spins. The Wilson number[2] W is given by[60,61]

$$W=\gamma e^{1/4}\pi^{-1/2}\approx 1.290\,268\,998, \tag{24}$$

where $\ln\gamma\approx 0.577\,215\,664\,902$ is Euler's constant. Setting $N=N_A$, Avogadro's number, one obtains from Eqs. (23) and (24) the electronic specific heat coefficient per mole of impurities:

$$\gamma(0)=\frac{\pi W R}{6T_K}=\frac{5.617\,14\text{ J/mol K}}{T_K}. \tag{25}$$

To characterize the T dependence of C_e, we utilized accurate numerical calculations using the Bethe ansatz by Jerez and Andrei.[59] The calculated $C_e(T)$ shows a maximum, $\max[C_e(T)/Nk_B]=0.177\,275$, which occurs at $T^{\max}/T_K=0.6928$. The calculations were fitted by the expressions

$$\frac{C_e(T)}{Nk_B}=f(t), \tag{26a}$$

$$\frac{C_e(T)}{Nk_BT/T_K}=g(t)\equiv\frac{f(t)}{t}, \tag{26b}$$

$$f(t)=\left(\frac{\pi W}{6}\right)\frac{t(1+a_1t+a_2t^2+a_3t^3+a_4t^4)}{1+a_5t+a_6t^2+a_7t^3+a_8t^4+a_9t^5}, \tag{26c}$$

where $t\equiv T/T_K$ and the coefficients a_n for the two types of fits are given in Table IV for the fitting range $0.001\leqslant t$

TABLE IV. Coefficients a_n in Eq. (26c) in the fits to the theoretical prediction for the specific heat vs temperature of the $S=1/2$ Kondo model by Jerez and Andrei (Ref. 59).

a_n	$C(T)$ fit	$C(T)/T$ fit
a_1	9.1103933	6.8135534
a_2	30.541094	21.718636
a_3	2.1041608	2.3491812
a_4	0.0090613513	0.017533911
a_5	9.1164094	6.8158433
a_6	36.143206	27.663307
a_7	67.91795	48.229552
a_8	53.509135	40.216156
a_9	1.7964377	2.4863342

$\leqslant 100$. Equations (26) incorporate the zero-temperature limit in Eqs. (23)–(25). The maximum (rms) deviations of the $C_e(T)$ fit from the calculated numerical data are 0.011% (0.0035%) for $0.001 \leqslant t \leqslant 3$ and 0.031% (0.021%) for $3 \leqslant t \leqslant 10$ but then progressively deteriorate to 0.48% (0.14%) in the region $10 \leqslant t \leqslant 92$. The corresponding deviations for the $C_e(T)/T$ fit are 0.0044% (0.000 91%), 0.031% (0.017%), and 5.1% (1.6%).

The experimental $C_e(T)/T$ data for LiV_2O_4 sample 3 were least-squares fitted from 1.2 to 5 K by Eqs. (26b) and (26c),[62] yielding T_K, and then $\gamma(0)$ from Eq. (25):

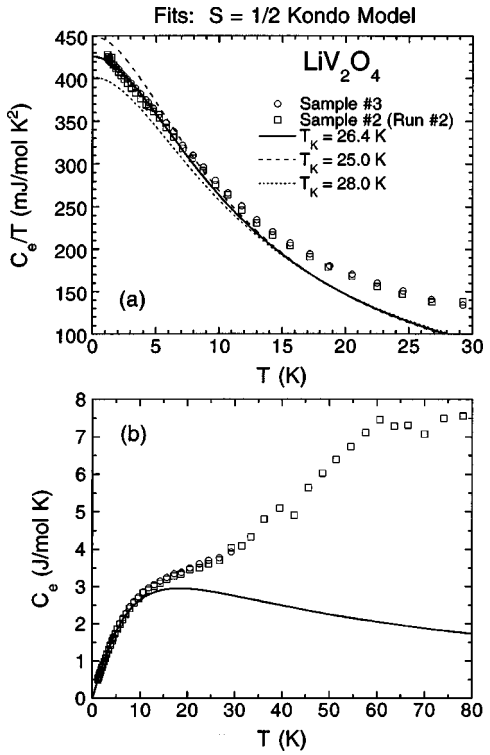

FIG. 13. (a) Electronic specific heat divided by temperature $C_e(T)/T$ data for LiV_2O_4 samples 2 (run 2) and 3 below 30 K (open symbols) and a fit (solid curve) of the data for sample 3 by the $S=1/2$ Kondo model, Eqs. (26b) and (26c), for a Kondo temperature $T_K=26.4$ K. Shown for comparison are the predictions for $T_K=25.0$ K (long-dashed curve) and 28.0 K (short-dashed curve). (b) The same data and the fit with $T_K=26.4$ K in a plot of C_e vs T up to 80 K.

TABLE V. Coefficients c_n in Eq. (28) for the high-temperature series expansion for the magnetic specific heat of the B sublattice of the spinel structure, for the indicated values of spin S.

n	$S=1/2$	$S=1$
1	$-1/2$	$-13/6$
2	$-23/16$	-3
3	65/48	715/36
4	1183/768	$-4421/324$
5	$-18971/7680$	$-670741/6480$

$$T_K = 26.4(1)\ \text{K}, \quad \gamma(0) = 426(2)\ \text{mJ/mol K}^2. \tag{27}$$

The fit is shown in Fig. 13 as the solid curves. For comparison, also shown in Fig. 13(a) are the predictions for $T_K=25$ K and 28 K. Unfortunately, despite the good agreement of the theory for $T_K=26.4$ K with our measured $C_e(T)$ at low T, the $S=1/2$ Kondo model prediction for $\chi(T)$ qualitatively disagrees with the observed temperature dependence at low T.[5] This difficulty of self-consistently fitting the $C_e(T)$ and $\chi(T)$ data is a problem we have encountered in all our attempts so far to fit our data for both measurements over any extended temperature range by existing theory (see also the next section).

D. Local moment high-temperature description

As discussed above, the $\chi(T)$ data for LiV_2O_4 suggest that at high temperatures a local moment description in which the moments are antiferromagnetically coupled with Weiss temperature $\theta \sim -30$ to -60 K may be applicable.[4,5] Accordingly, we have calculated the magnetic specific heat $C_m(T)$ for localized moments on the octahedral (B) sublattice of the $A[B_2]O_4$ spinel structure assuming nearest-neighbor AF Heisenberg interactions using the general high-temperature series expansion (HTSE) results of Rushbrooke and Wood.[63] The Hamiltonian is $\mathcal{H}=J\Sigma_{\langle ij\rangle}\boldsymbol{S}_i\cdot\boldsymbol{S}_j$, where the sum is over all exchange bonds and the exchange constant $J>0$ corresponds to AF interactions. In terms of this Hamiltonian, $\theta=-zJS(S+1)/3$, where $z=6$ is the coordination number for the B sublattice of the spinel structure. The above range of θ then gives $J/k_B=20$–40 K assuming $S=1/2$. The general HTSE prediction is[63]

$$\frac{C_m(T)}{Nk_B} = \frac{z[S(S+1)]^2}{6t^2}\left[1+\sum_{n=1}^{n^{\max}}\frac{c_n(S)}{t^n}\right], \tag{28}$$

where $t \equiv k_BT/J$ and the coefficients c_n depend in general on the spin-lattice structure in addition to S. The coefficients c_n for the B sublattice of the spinel structure with $S=1/2$ and $S=1$ up to the maximum available $n^{\max}=5$ are given in Table V. The predictions for C_m versus scaled temperature $k_BT/[JS(S+1)]$ with $n^{\max}=5$ are very similar for $S=1/2$ and $S=1$. A comparison of the $C_m(T)$ predictions for $n^{\max}=0$ to 5 indicates that the calculations for $n^{\max}=5$ are accurate for $k_BT/[JS(S+1)] \gtrsim 2.5$, a T range with a lower limit slightly above the temperatures at which broad maxima occur.

In Fig. 14 the HTSE prediction of $C_m(T)$ for the B sublattice of the spinel structure with $n^{\max}=5$, $S=1/2$, and

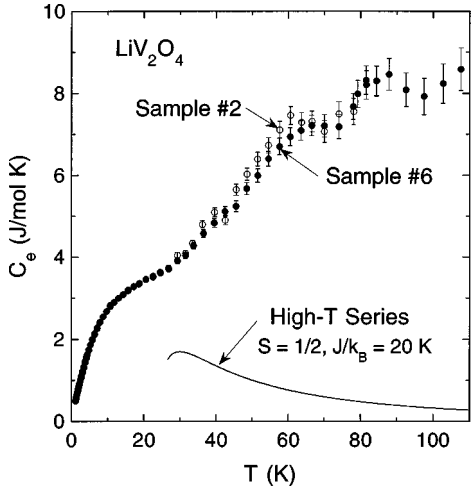

FIG. 14. Comparison of the high-temperature series expansion prediction for the magnetic specific heat $C_m(T)$ of the B sublattice of the $A[B_2]O_4$ spinel structure assuming $S=1/2$, $J/k_B=20$ K, and $n^{max}=5$, given by Eq. (28) with c_n coefficients in Table V, with the experimental $C_e(T)$ data for LiV_2O_4 sample 2 (run 2) and sample 6 from Fig. 4(a).

$J/k_B=20$ K in Eq. (28) is compared with the experimental $C_e(T)$ data for LiV_2O_4 samples 2 and 6 from Fig. 4(a). The HTSE $C_m(T)$ has a much lower magnitude than the data and a qualitatively different temperature dependence. From Eq. (28), changing J just scales the curve with T. Thus the local moment picture is in severe disagreement with our $C_e(T)$ measurements, despite the excellent agreement between the corresponding HTSE $\chi(T)$ prediction and the $\chi(T)$ data from 50–100 K to 400 K.[4,5]

VI. SUMMARY AND CONCLUDING REMARKS

We have presented $C_p(T)$ data for LiV_2O_4 sample 6 which extend our previous measurements[4] up to 108 K. We have also presented $C_p(T)$ data for the isostructural superconducting compound $LiTi_2O_4$ ($T_c=11.8$ K) up to 108 K which complement our earlier data[4] on the isostructural nonmagnetic insulator $Li_{4/3}Ti_{5/3}O_4$. We concluded here that the lattice contribution $C^{lat}(T)$ to $C_p(T)$ for $LiTi_2O_4$ provides the more reliable estimate of the $C^{lat}(T)$ for LiV_2O_4, and we then extracted the electronic contribution $C_e(T)$ to $C_p(T)$ of LiV_2O_4 from 1.2 to 108 K. Inelastic neutron scattering measurements of the lattice dynamics and spin excitations would be very useful in interpreting the measurements presented here. It will be important to determine whether or not there exist significant differences in the lattice dynamics of LiV_2O_4 and $LiTi_2O_4$; in our data analyses and modeling, we have assumed that these compounds are similar in this respect.

For two high-magnetic-purity LiV_2O_4 samples 3 and 6, the electronic specific heat coefficients $\gamma(T)\equiv C_e(T)/T$ were found to be $\gamma(1\,\mathrm{K})=0.42$ and 0.43 J/mol K^2, respectively. To our knowledge, these values are significantly larger than previously reported for any metallic transition-metal compound.[64] For $LiTi_2O_4$, we found $\gamma=0.018$ J/mol K^2. $\gamma(T)$ of LiV_2O_4 decreases rapidly with increasing temperature from 4 to 30 K and then decreases much more slowly

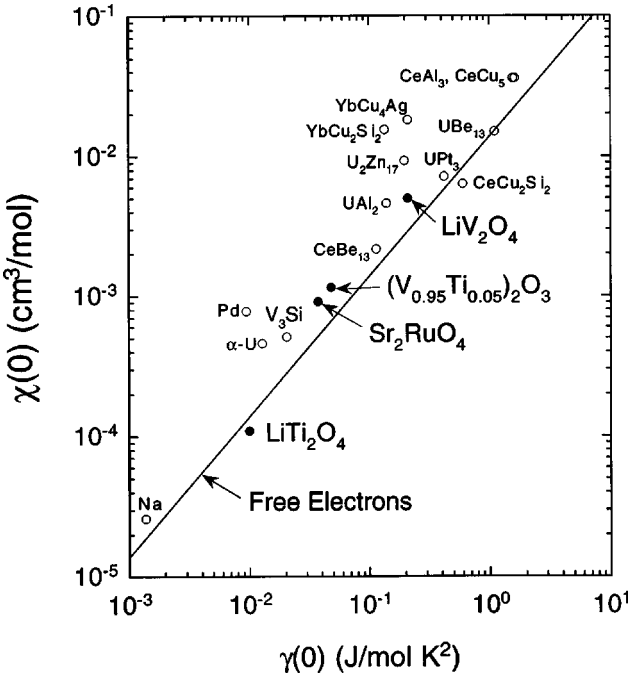

FIG. 15. Log-log plot of the magnetic susceptibility $\chi(0)$ vs electronic specific heat coefficient $\gamma(0)$ at zero temperature for a variety of *f*-electron heavy-fermion and intermediate-valence compounds compiled from the literature (after Ref. 64). The plot also includes data for several elemental and/or *d*-electron metals and our data point for LiV_2O_4. Here, a ''mol'' in the axis labels refers to a mole of transition-metal atoms for the *d*-metal compounds and to a mole of *f*-electron atoms for compounds containing lanthanide or actinide atoms. The straight line corresponds to a Wilson ratio $R_W=1$ for quasiparticles with spin $S=1/2$ and g factor $g=2$, which is also the Wilson ratio for a free electron Fermi gas.

from a value of 0.13 J/mol K^2 at 30 K to 0.08 J/mol K^2 at 108 K. Even these latter two γ values are exceptionally large for a metallic *d*-electron compound. The temperature dependences of γ, χ, the low-T resistivity, and the ^{7}Li NMR properties are remarkably similar to those of the heaviest-mass *f*-electron heavy-fermion compounds.[1] In a plot of $\chi(0)$ versus $\gamma(0)$, the data point for LiV_2O_4 sits amid the cluster formed by the *f*-electron heavy-fermion and intermediate-valence compounds as shown in Fig. 15,[65] where several data for elemental metals, the A-15 superconductor V_3Si ($T_c=17$ K),[66,67] and superconducting and/or metallic *d*-metal oxides $LiTi_2O_4$ ($T_c\leqslant 13.7$ K),[14] Sr_2RuO_4 ($T_c=1$ K),[68] and $(V_{0.95}Ti_{0.05})_2O_3$,[69] are also included for comparison.

From our theoretical modeling in Sec. V, Fermi liquid models and the $S=1/2$ Kondo model (with a Fermi liquid ground state) are capable of describing our $C_e(T)$ data for LiV_2O_4 from 1 K up to $\sim$10 K, although the magnitudes of the derived parameters remain to be understood theoretically. The localized moment model in Sec. V D failed both qualitatively and quantitatively to describe the data. None of the models we used can account for the additional contribution to $C_e(T)$ at higher temperatures, from $\sim$10 K up to our high-temperature limit of 108 K, which appears to be distinct from the contribution beginning at much lower T and could arise from orbital,[70,71] charge, and/or spin[72,73] excitations. The crystalline electric field and/or the spin-orbit interaction may

produce some energy level structure which is thermally accessible within our temperature range.[74] Conventional band structure effects cannot give rise to our results.[75]

As is well known for conventional metals, the electron-phonon interaction increases γ by the factor $(1+\lambda)$, where λ is the electron-phonon coupling constant, but does not affect χ; i.e., $\mathcal{D}^*(E_F) \rightarrow \mathcal{D}^*(E_F)(1+\lambda)$ in Eq. (10a). One can correct the observed Wilson ratio for electron-phonon interactions by multiplying the observed value by $(1+\lambda)$.[76] The electron-phonon interaction is not taken into account in any of the analyses or modeling we have done. This correction would have had a significant quantitative impact on our analyses if we used, e.g., $\lambda \approx 0.7$ as in $LiTi_2O_4$ (Refs. 20 and 28); most previous analyses of the specific heats of other (f-electron) HF compounds also did not take the electron-phonon interaction into account.[1]

From our combined specific heat and thermal expansion measurements on the same sample 6 of LiV_2O_4 from 4.4 to 108 K, we derived the Grüneisen parameter $\Gamma(T)$ which shows a dramatic enhancement below ~ 25 K as the compound crosses over from the quasilocal moment behavior at high temperatures to the low-temperature Fermi liquid regime, confirming the discovery of Chmaissem *et al.* from neutron diffraction measurements.[8] Our estimated extrapolated value of the electronic Grüneisen parameter $\Gamma_e(0)$ is about 11.4, which is intermediate between values for conventional metals and for f-electron heavy-fermion compounds. This large value indicates a much stronger dependence of the mass-enhanced density of states on the volume of the system than simply due to the decrease in the Fermi energy with increasing volume as in the quasifree electron picture. In the f-electron HF systems, the large $\Gamma_e(0)$ values are thought to arise from a strongly volume-dependent hybridization of the f-electron orbitals with those of the conduction electrons.[36,77] In the present case of LiV_2O_4, the origin of the large $\Gamma_e(0)$ is unclear.

It is conceivable that the same mechanism is responsible for the heavy-fermion behavior in LiV_2O_4 as in the f-electron heavy-fermion systems if one of the 1.5 d electrons/V atom is localized on each V atom due to electron correlation effects and crystalline electric field orbital energy level structure,[78] and if the orbital occupied by the localized electron is hybridized only weakly with the conduction-electron states. That such localization can occur in similar systems is supported by calculations for the d^1 compound $NaTiO_2$.[79] Additional scenarios for the heavy-fermion behavior mechanism(s) are given by Kondo and co-workers[4,5] involving the geometric frustration for AF ordering within the V sublattice and/or low-lying coupled dynamical orbital-charge-spin excitations. Further experimental and theoretical investigations of the physical properties of LiV_2O_4 may thus reveal interesting new physics which may also allow a deeper understanding of the f-electron heavy-fermion class of materials.

ACKNOWLEDGMENTS

We are indebted to F. Izumi for helpful communications regarding the Rietveld analyses and to A. Jerez and N. Andrei for providing high-accuracy numerical values[59] of the magnetic susceptibility and specific heat of the $S=1/2$ Kondo model. We thank V. Antropov, F. Borsa, O. Chmaissem, J. B. Goodenough, R. J. Gooding, B. N. Harmon, J. D. Jorgensen, M. B. Maple, and A. J. Millis for helpful discussions and correspondence, and V. Antropov and B. N. Harmon for communicating to us the results of their unpublished band structure calculations for LiV_2O_4. Ames Laboratory is operated for the U.S. Department of Energy by Iowa State University under Contract No. W-7405-Eng-82. This work was supported by the Director for Energy Research, Office of Basic Energy Sciences.

[1] For reviews, see G. R. Stewart, Rev. Mod. Phys. **56**, 755 (1984); A. C. Hewson, *The Kondo Problem to Heavy Fermions* (Cambridge University Press, Cambridge, England 1993).
[2] K. G. Wilson, Rev. Mod. Phys. **47**, 773 (1975).
[3] D. B. Rogers, J. L. Gillson, and T. E. Gier, Solid State Commun. **5**, 263 (1967).
[4] S. Kondo, D. C. Johnston, C. A. Swenson, F. Borsa, A. V. Mahajan, L. L. Miller, T. Gu, A. I. Goldman, M. B. Maple, D. A. Gajewski, E. J. Freeman, N. R. Dilley, R. P. Dickey, J. Merrin, K. Kojima, G. M. Luke, Y. J. Uemura, O. Chmaissem, and J. D. Jorgensen, Phys. Rev. Lett. **78**, 3729 (1997).
[5] S. Kondo, D. C. Johnston, and L. L. Miller, preceding paper, Phys. Rev. B **59**, 2604 (1999).
[6] A. V. Mahajan, R. Sala, E. Lee, F. Borsa, S. Kondo, and D. C. Johnston, Phys. Rev. B **57**, 8890 (1998).
[7] J. Merrin, Y. Fudamoto, K. M. Kojima, M. Lardin, G. M. Luke, B. Nachumi, Y. J. Uemura, S. Kondo, and D. C. Johnston (unpublished).
[8] O. Chmaissem, J. D. Jorgensen, S. Kondo, and D. C. Johnston, Phys. Rev. Lett. **79**, 4866 (1997).
[9] Y. Ueda, N. Fujiwara, and H. Yasuoka, J. Phys. Soc. Jpn. **66**, 778 (1997).
[10] M. Onoda, H. Imai, Y. Amako, and H. Nagasawa, Phys. Rev. B **56**, 3760 (1997).
[11] N. Fujiwara, Y. Ueda, and H. Yasuoka, Physica B **237-238**, 59 (1997).
[12] N. Fujiwara, H. Yasuoka, and Y. Ueda, Phys. Rev. B **57**, 3539 (1998).
[13] B. Reuter and J. Jaskowsky, Angew. Chem. **72**, 209 (1960); Ber. Bunsenges. Phys. Chem. **70**, 189 (1966).
[14] D. C. Johnston, J. Low Temp. Phys. **25**, 145 (1976).
[15] A. Deschanvres, B. Raveau, and Z. Sekkal, Mater. Res. Bull. **6**, 64 (1971).
[16] R. J. Cava, D. W. Murphy, S. Zahurak, A. Santoro, and R. S. Roth, J. Solid State Chem. **53**, 64 (1984).
[17] M. Dalton, I. Gameson, A. R. Armstrong, and P. P. Edwards, Physica C **221**, 149 (1994).
[18] D. C. Johnston, H. Prakash, W. H. Zachariasen, and R. Viswanathan, Mater. Res. Bull. **8**, 777 (1973).
[19] M. R. Harrison, P. P. Edwards, and J. B. Goodenough, Philos. Mag. B **52**, 679 (1985).
[20] J. M. Heintz, M. Drillon, R. Kuentzler, Y. Dossmann, J. P. Kappler, O. Durmeyer, and F. Gautier, Z. Phys. B **76**, 303 (1989).

[21] D. P. Tunstall, J. R. M. Todd, S. Arumugam, G. Dai, M. Dalton, and P. P. Edwards, Phys. Rev. B **50**, 16 541 (1994).
[22] T. Inukai, T. Murakami, and T. Inamura, Thin Solid Films **94**, 47 (1982).
[23] F. Bertaut and A. Durif, C.R. Acad. Sci. (Paris) **236**, 212 (1953).
[24] U. Zülicke and A. J. Millis, Phys. Rev. B **51**, 8996 (1995).
[25] F. Izumi, in *The Rietveld Method*, edited by R. A. Young (Oxford University Press, Oxford, 1993), Chap. 13.
[26] C. A. Swenson, Phys. Rev. B **53**, 3669 (1996).
[27] C. A. Swenson, in *Thermal Expansion of Solids*, edited by C. Y. Ho, CINDAS Data Series on Material Properties (American Society of Metals, Metals Park, OH, 1998), Chap. 8.
[28] R. W. McCallum, D. C. Johnston, C. A. Luengo, and M. B. Maple, J. Low Temp. Phys. **25**, 177 (1976).
[29] E. S. R. Gopal, *Specific Heats at Low Temperatures* (Plenum, New York, 1966).
[30] For a review, see T. H. K. Barron, J. G. Collins, and G. K. White, Adv. Phys. **29**, 609 (1980).
[31] G. D. Khattak, P. H. Keesom, and S. P. Faile, Phys. Rev. B **18**, 6181 (1978).
[32] U. Roy, K. Petrov, I. Tsolovski, and P. Peshev, Phys. Status Solidi A **44**, K25 (1977).
[33] F. Birch, in *Handbook of Physical Constants*, edited by S. P. Clark, Jr. (Geological Society of America, New York, 1966), Sec. 7, pp. 129–136.
[34] M. B. Kruger, J. H. Nguyen, W. Caldwell, and R. Jeanloz, Phys. Rev. B **56**, 1 (1997).
[35] R. M. Hazen and H. Yang, Science **277**, 1965 (1997).
[36] For a review, see A. de Visser, J. J. M. Franse, and J. Flouquet, Physica B **161**, 324 (1989).
[37] C. Kittel, *Introduction to Solid State Physics*, 4th ed. (Wiley, New York, 1971), Chap. 7.
[38] C. J. Pethick and G. M. Carneiro, Phys. Rev. A **7**, 304 (1973).
[39] C. J. Pethick, D. Pines, K. F. Quader, K. S. Bedell, and G. E. Brown, Phys. Rev. Lett. **57**, 1955 (1986).
[40] G. Baym and C. Pethick, *Landau Fermi Liquid Theory* (John Wiley & Sons, New York, 1991).
[41] J. R. Engelbrecht and K. S. Bedell, Phys. Rev. Lett. **74**, 4265 (1995).
[42] A. Auerbach and K. Levin, Phys. Rev. Lett. **57**, 877 (1986); Phys. Rev. B **34**, 3524 (1986).
[43] A. J. Millis, Phys. Rev. B **36**, 5420 (1987).
[44] A. J. Millis and P. A. Lee, Phys. Rev. B **35**, 3394 (1987).
[45] G. R. Stewart, Z. Fisk, J. O. Willis, and J. L. Smith, Phys. Rev. Lett. **52**, 679 (1984).
[46] W. Trinkl, U. Weilnhammer, S. Corsépius, T. Schreiner, E.-W. Scheidt, and G. R. Stewart, Phys. Rev. B **54**, 1163 (1996).
[47] A. Ishigaki and T. Moriya, J. Phys. Soc. Jpn. **65**, 376 (1996).
[48] M. Dalton, D. P. Tunstall, J. Todd, S. Arumugam, and P. P. Edwards, J. Phys.: Condens. Matter **6**, 8859 (1994).
[49] L. B. Ioffe and A. J. Millis, Phys. Rev. B **51**, 16 151 (1995).
[50] In the fit to the specific heat data by this theory in Ref. 4, r = const and $\alpha = 1$ were assumed.
[51] A. J. Millis (private communication).
[52] H. R. Krishna-murthy, J. W. Wilkins, and K. G. Wilson, Phys. Rev. B **21**, 1003 (1980).
[53] H. R. Krishna-murthy, J. W. Wilkins, and K. G. Wilson, Phys. Rev. B **21**, 1044 (1980).
[54] L. N. Oliveira and J. W. Wilkins, Phys. Rev. Lett. **47**, 1553 (1981).
[55] V. T. Rajan, J. H. Lowenstein, and N. Andrei, Phys. Rev. Lett. **49**, 497 (1982).
[56] V. T. Rajan, Phys. Rev. Lett. **51**, 308 (1983).
[57] H.-U. Desgranges and K. D. Schotte, Phys. Lett. **91A**, 240 (1992).
[58] A. M. Tsvelick and P. B. Wiegmann, Adv. Phys. **32**, 453 (1983).
[59] A. Jerez and N. Andrei (unpublished).
[60] N. Andrei and J. H. Lowenstein, Phys. Rev. Lett. **46**, 356 (1981).
[61] J. W. Rasul and A. C. Hewson, J. Phys. C **17**, 3337 (1984).
[62] The prediction of Rajan *et al.* (Refs. 54 and 55) for $C_e(T)$ of the $S = 1/2$ Kondo model was used to fit our low-T $C_p(T)$ data in our initial publication (Ref. 4), where we used a fit to digitized data from the theoretical plots. The digitized data were parametrized by $C_e(T) = [(0.8278\ \mathrm{J/mol\,K})(Lg + 3.959)]/[(Lg + 0.2510)^2 + 1.398]^{2.217}$, where $Lg \equiv \log_{10}(T/T_K)$.
[63] G. S. Rushbrooke and P. J. Wood, Mol. Phys. **1**, 257 (1958). Note that the definition of J in this paper is a factor of 2 smaller than ours. We determined the parameters in this paper corresponding to the B sublattice of the $A[B_2]O_4$ spinel structure to be $z = 6$, $p_1 = 2$, $p_2 = 2$, $p_3 = 0$, $p_4 = 2$, $p_5 = 12$, $q = 0$, $r = 2$, and $t = 0$.
[64] R. Ballou, E. Lelièvre-Berna, and B. Fåk, Phys. Rev. Lett. **76**, 2125 (1996).
[65] B. A. Jones *et al.*, Fig. 1 in P. A. Lee, T. M. Rice, J. W. Serene, L. J. Sham, and J. W. Wilkins, Comments Condens. Matter Phys. **12**, 99 (1986).
[66] A. Junod, J.-L. Staudenmann, J. Muller, and P. Spitzli, J. Low Temp. Phys. **5**, 25 (1971).
[67] J. P. Maita and E. Bucher, Phys. Rev. Lett. **29**, 931 (1972).
[68] Y. Maeno, K. Yoshida, H. Hashimoto, S. Nishizaki, S. Ikeda, M. Nohara, T. Fujita, A. P. Mackenzie, N. E. Hussey, J. G. Bednorz, and F. Lichtenberg, J. Phys. Soc. Jpn. **66**, 1405 (1997).
[69] D. B. McWhan, J. P. Remeika, T. M. Rice, W. F. Brinkman, J. P. Maita, and A. Menth, Phys. Rev. Lett. **27**, 941 (1971).
[70] M. Takigawa, E. T. Ahrens, and Y. Ueda, Phys. Rev. Lett. **76**, 283 (1996).
[71] W. Bao, C. Broholm, G. Aeppli, P. Dai, J. M. Honig, and P. Metcalf, Phys. Rev. Lett. **78**, 507 (1997).
[72] J. B. Silva, W. L. C. Lima, W. C. Oliveira, J. L. N. Mello, L. N. Oliveira, and J. W. Wilkins, Phys. Rev. Lett. **76**, 275 (1996).
[73] N. Andrei and A. Jerez, Phys. Rev. Lett. **74**, 4507 (1995).
[74] R. J. Radwański (unpublished).
[75] V. Antropov and B. N. Harmon (unpublished).
[76] P. Fulde, J. Keller, and G. Zwicknagl, in *Solid State Physics*, edited by H. Ehrenreich and D. Turnbull (Academic Press, San Diego, 1988), Vol. 41, pp. 1–150.
[77] A. S. Edelstein and N. C. Koon, Solid State Commun. **48**, 269 (1983); for a review, see P. Thalmeier, J. Magn. Magn. Mater. **76&77**, 299 (1988).
[78] J. B. Goodenough (private communication).
[79] S. Yu. Ezhov, V. I. Anisimov, H. F. Pen, D. I. Khomskii, and G. A. Sawatzky, Europhys. Lett. **44**, 491 (1998).